remote sensing

MDPI

Article

Mapping Coastal Aquaculture Ponds of China Using Sentinel SAR Images in 2020 and Google Earth Engine

Peng Tian [1,2], Yongchao Liu [1,2,3], Jialin Li [1,2,3], Ruiliang Pu [4], Luodan Cao [1], Haitao Zhang [1], Shunyi Ai [1] and Yunze Yang [5,*]

1 Department of Geography and Spatial Information Techniques, Ningbo University, Ningbo 315211, China
2 Donghai Academy, Ningbo University, Ningbo 315211, China
3 Collaborative Innovation Center for Land and Marine Spatial Utilization and Governance Research, Ningbo University, Ningbo 315211, China
4 School of Geosciences, University of South Florida, Tampa, FL 33620-5250, USA
5 School of Civil Engineering and Environment, Ningbo University, Ningbo 315211, China
* Correspondence: 2011087076@nbu.edu.cn

Abstract: Aquaculture has enormous potential for ensuring global food security and has experienced rapid growth globally. Thus, the accurate monitoring and mapping of coastal aquaculture ponds is necessary for the sustainable development and efficient management of the aquaculture industry. Here, we developed a map of coastal aquaculture ponds in China using Google Earth Engine (GEE) and the ArcGIS platform, Sentinel-1 SAR image data for 2020, the Sentinel-1 Dual-Polarized Water Index (SDWI), and water frequency obtained by identifying the special object features of aquaculture ponds and postprocessing interpretation. Our map had an overall accuracy of 93%, and we found that the coastal aquaculture pond area in China reached 6937 km^2 in 2020. The aquaculture pond area was highest in Shandong, Guangdong, and Jiangsu Provinces, and at the city level, Dongying, Binzhou, Tangshan, and Dalian had the most aquaculture pond area. Aquaculture ponds had spatial heterogeneity; the aquaculture pond area in north China was larger than in south China and seaside areas had more pond area than inland regions. In addition, aquaculture ponds were concentrated near river estuaries, coastal plains, and gulfs, and were most dense in the Huang-Huai-Hai Plain and Pearl River Delta. We showed that GEE cloud processing and ArcGIS local processing could facilitate the classification of coastal aquaculture ponds, which can be used to inform and improve decision-making for the spatial optimization and intelligent monitoring of coastal aquaculture, with certain potential for spatial migration.

Keywords: aquaculture ponds; spatial distribution; Sentinel-1 SAR images; Google Earth Engine; coastal area of China

check for updates

Citation: Tian, P.; Liu, Y.; Li, J.; Pu, R.; Cao, L.; Zhang, H.; Ai, S.; Yang, Y. Mapping Coastal Aquaculture Ponds of China Using Sentinel SAR Images in 2020 and Google Earth Engine. *Remote Sens.* **2022**, *14*, 5372. https://doi.org/10.3390/rs14215372

Academic Editors: Jiayi Pan, Hongsheng Zhang, Bo Huang and Adam T. Devlin

Received: 5 September 2022
Accepted: 25 October 2022
Published: 26 October 2022

1. Introduction

Since the 1970s, global aquaculture production has grown rapidly [1]. Along with a rapidly growing world population, aquaculture plays an increasingly significant role in the supply of high-quality animal protein [2]. Numerous studies have shown that the aquaculture industry is developing at a high speed and can help achieve sustainable development goals in the 2030 United Nations Agenda of for Sustainable Development [3,4], such as reducing poverty, eliminating hunger, food security, improving nutritional status, and promoting, protecting, and utilizing oceans and marine resource sustainably to boost sustainable development [5]. With the emergence of the aquaculture industry, aquaculture techniques and experience have been continuously updated and communicated [6], which has promoted the growth of global aquaculture products. A series of environmental problems, such as the destruction of natural wetlands [7], the degradation of ecosystem stability [8], and water pollution [9], have been unavoidably brought by the rapid expansion of aquaculture ponds [10], which is especially true for the large-scale construction of dense aquaculture ponds in coastal areas [11,12].

Cultivated land, grassland, and forest-centered food production departments have carried out extensive studies [13,14], but studies on the aquaculture industry have just begun. In particular, rapid population growth has considerably increased the demand for aquaculture products, so it is rather essential to strengthen the sustainable and scientific management of aquaculture [15]. The primary challenge in this management is a clear understanding of aquaculture pond area and their spatial distribution characteristics [16]. Aquaculture data are usually acquired by reviewing statistical data, which is not timely or frequent. Traditional field investigations can accurately identify and measure aquaculture ponds, but field investigations consume a lot of manpower and financial resources [17]. Remote sensing technologies, which can have highly frequent observations at large spatial scales, can be used to map aquaculture ponds and are an effective tool for accurately and rapidly monitoring the spatial–temporal distribution and development of aquaculture ponds [15,18].

Optical sensors and radar sensors have been extensively used to map aquaculture ponds (Table A1) [19–21]. These sensors mainly include Landsat TM/ETM+/OLI, Worldview series, Spot series, QuickBird, ASTER, IKONOS, China GF image series, TerraSAR-X, Sentinel-1, and Sentinel-2 [18,22,23]. Optical remote sensing images from these platforms, which provide long time-series data, have been widely utilized for the long-term monitoring of regional aquaculture ponds [10,24,25]. For instance, Stiller et al. [26] used Landsat TM/ETM+/OLI images to investigate the temporal–spatial variation characteristics of regional aquaculture ponds during 1984–2016 in the Yellow River Delta and Pearl River Delta in China. Duan et al. [24] explored the dynamic variation in large-scale aquaculture ponds in the Jiangsu Province of China during 1988–2018 using TM/OLI images. In general, the spatial resolution of Landsat images is 30 m, while aquaculture ponds in remote sensing images are so small that they cannot be accurately identified using coarse-resolution satellite images [10,27]. Hence, medium- and high-resolution satellite images have been used to map aquaculture ponds in recent years [15,23], but high-resolution images have a low temporal resolution and are costly, which complicates large-scale aquaculture pond mapping [15]. Sentinel images not only have a relatively long data record (2014-) and high spatial resolution (10 m) but they also have strong practical operability [27,28]. For example, Ottinger et al. [23] accurately mapped coastal aquaculture ponds in Asia using Sentinel-1 and Sentinel-2 images. Sun et al. [16] mapped the spatial distribution of coastal aquaculture ponds in Vietnam in 2020 using Sentinel-1 data.

The Sentinel-1 satellite carries synthetic aperture radar (SAR) sensors, which can relieve the influences of cloud layers on satellite images since its wavebands can penetrate cloud layers, have high temporal and spatial resolutions, and are provided free-of-charge [23,29,30]. Given the weak backscattering of conventional SAR on water surfaces, water bodies can be effectively identified using SAR images according to the echo intensity of radar waves [15]. Nowadays, Sentinel-1 SAR images have been widely applied for the identification of water bodies [31], with favorable applicability and operability in large-scale continuous mapping and monitoring research, such as the monitoring of spatiotemporal variations in water bodies (e.g., aquaculture ponds, surface floods, rivers, lakes, and reservoirs) [32–34]. Aquaculture ponds are shallow water surfaces surrounded by dikes, which can be scanned and monitored using radar images according to the high contrast between a smooth water surface (low radar backscattering) and a coarse non-water surface (high radar backscattering) [23,35]. Therefore, Sentinel-1 SAR images are valuable for identifying and monitoring aquaculture ponds. Presently, the GEE online platform is widely used in aquaculture pond mapping [34], which can save a large amount of time and energy in image acquisition and data processing. Our main workflow included image acquisition, water index construction, the acquisition of potential aquaculture ponds, the object feature screening of aquaculture ponds, space mapping, and accuracy evaluation, all of which was conducted using GEE [16,34]. However, various sources of error, such as salt pans, seasonal water bodies, waste fishponds, and tidal flat wetlands, can be misclassified as aquaculture ponds [36]. In summary, the efficient data processing capacity of GEE should be first used to classify aquaculture ponds to save time and energy. Offline refined extraction should also be conducted using the ArcGIS platform or other data processing software, so as to construct online and offline aquaculture pond extraction methods and determine the most accurate mapping of large-scale aquaculture ponds.

China has the longest history of aquaculture. As the world's largest aquaculture country, the total aquaculture area of China was 70,361 km^2 in 2020, 30,369 km^2 of which was aquaculture ponds, accounting for 43.16% of the total aquaculture area [37]. Aquaculture ponds play significant roles in ensuring food security and providing high-quality proteins. Here, we used cloud-based GEE and local ArcGIS methods to identify and map coastal aquaculture. The main objectives of our study were to: (1) construct an online–offline combined aquaculture pond extraction method to effectively map coastal aquaculture ponds; (2) compare the similarities and differences between the aquaculture ponds we identified using this method and those in the currently popular land cover (LC) datasets; and (3) figure out the possible error sources in the extraction work of aquaculture ponds. Our resultant maps can improve our knowledge of the location and spatial extent of China's coastal aquaculture ponds, and our method can be applied effectively in other large areas to map and manage aquaculture ponds.

2. Materials and Methods

2.1. Study Area

Given China's long history of coastal aquaculture, many aquaculture ponds (Figure 1) are distributed along China's 18,000 km of coastline. The coastal areas are mainly used for fish, shellfish, algae, shrimp, and crab farming. For example, there are intensive breeding ponds in the Pearl River Delta and many crab ponds in Sanmen Bay, Zhejiang Province. The coastal aquaculture ponds in China have different shape and structural characteristics due to the differences in their geographical locations (plains, hills, estuaries, deltas, mudflats, and gulfs) and levels of socioeconomic development [17,18]. Our study took China's coast as the research area, which involved 260 counties, 12 provinces, and 2 special administrative regions with an area of 278,764 km^2. Coastal aquaculture ponds presented significant spatial agglomeration characteristics and large-area spatial network structural characteristics. In addition, some isolated aquaculture ponds are distributed along coastal zones, whose area is so small as not to be effectively identified. In our study, therefore, we aimed to map aquaculture ponds that were larger than 0.005 km^2. Based on previous studies and field surveys, the coastal aquaculture ponds in China are basically wet during April–October and are relatively stable water bodies [18,24]. In other months, however, the aquaculture ponds are dry, and fishermen will perform desilting, sun drying, and sterilization activities.

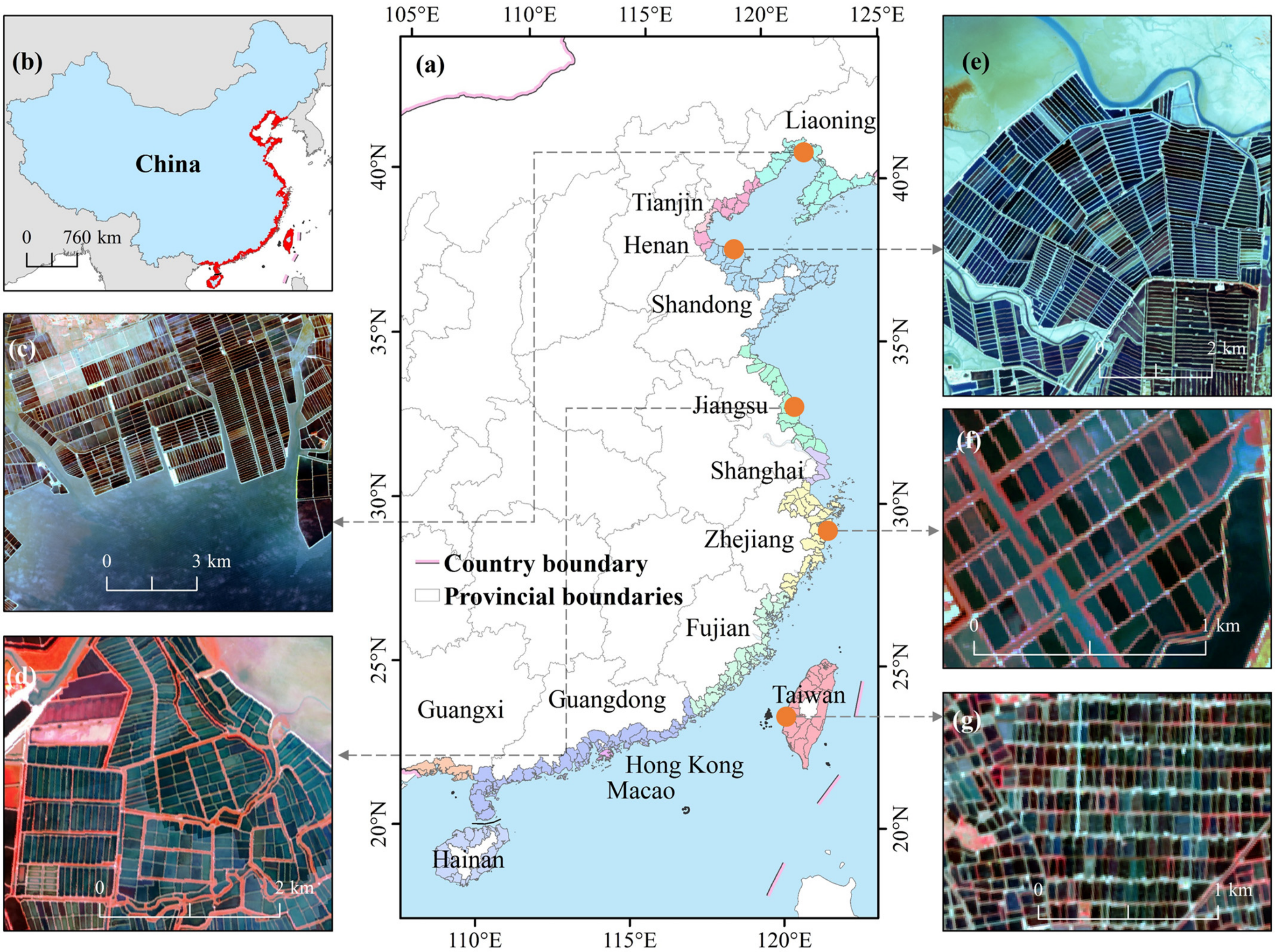

Figure 1. China's coast and images of typical aquaculture ponds. (**a**) Geographical location of the study area; (**b**) the location of the study area in China; (**c**) aquaculture ponds on the Liaoning estuary delta plain (Sentinel-2 images using R8-G4-B3 band combinations); (**d**) aquaculture ponds on the coastal plain of Jiangsu; (**e**) tidal flats in Shandong; (**f**) aquaculture ponds near Zhejiang Bay; and (**g**) aquaculture ponds in the landside plains of Taiwan.

2.2. Dataset

2.2.1. Sentinel-1 Image and Processing

Sentinel-1, a full-time and all-weather radar-imaging system that was formally launched in October of 2014, is characterized by dual polarization, a short revisit cycle, and rapid product production [30]. We used all Sentinel-1 data covering our study area in 2020 (1 April to 31 October) stored in GEE, which included 1415 dual-polarized (VV + VH) images (Figure 2) in the interferometric wide swath and ground range detection (GRD) formats [35]. The spatial resolution of the dataset was 5 m × 20 m, its ground sampling range was 10 m, and all images were stored in the GEE platform. The Sentinel-1 SAR data on this platform were already preprocessed using Sentinel-1 toolbox from the European Space Agency (ESA), including thermal noise removal, radiometric calibration, and terrain correction [33].

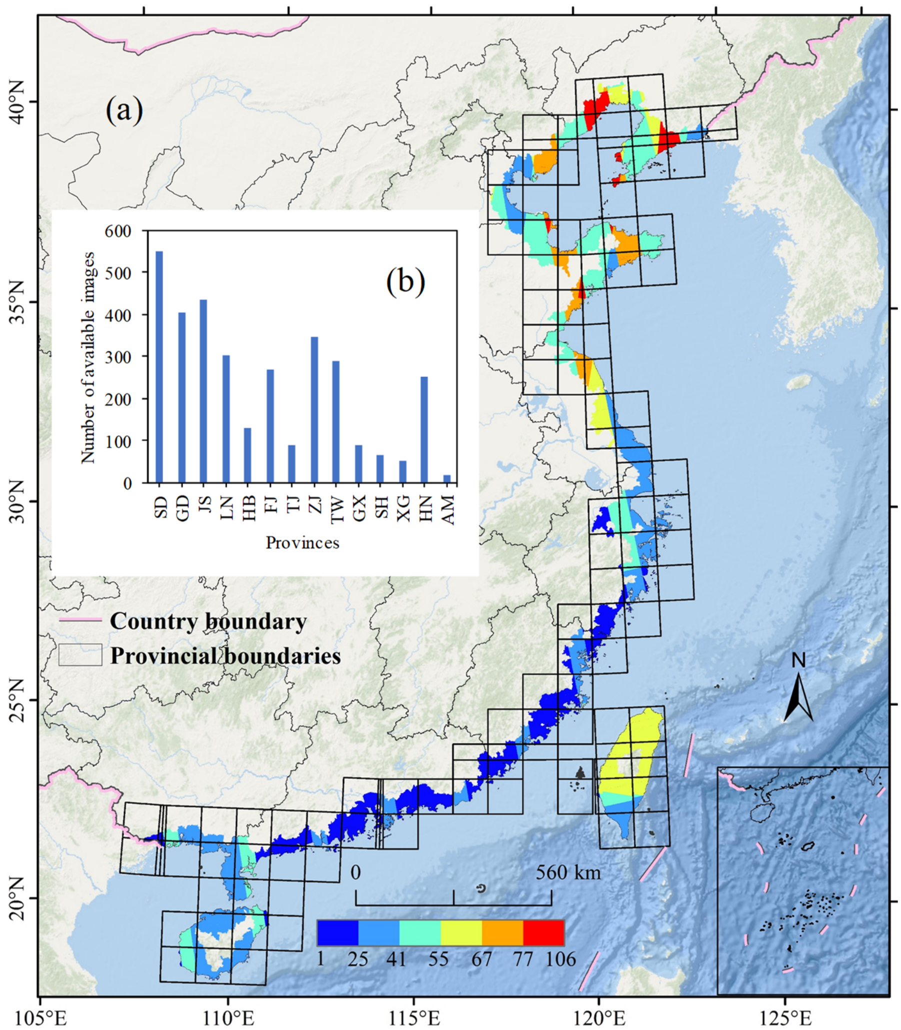

Figure 2. The number of available images in Sentinel-1 in the study area. (**a**) Availability of images in the entire study area; (**b**) number of available images in each province.

2.2.2. Auxiliary Data

(1) DEM. The Shuttle Radar Topography Mission (SRTM) digital elevation data on GEE platform were chosen as the DEM data. The SRTM V3 product (SRTM Plus) was provided by NASA JPL. The spatial resolution of SRTM is 30 m, the horizontal accuracy of its C-band and X-band are both 20 m, and the elevation accuracy of its C-band and X-band are 20 m and 4 m, respectively. This dataset was gap-filled using open-source data (ASTER GDEM2, GMTED2010, and NED), ensuring the data's accuracy and applicability. According to Duan et al. [17], coastal aquaculture ponds are mainly distributed in coastal lowlands with an elevation of <20 m, so we performed elevation screening of the images (DEM < 20 m) before extracting the aquaculture ponds.

(2) JRC yearly water classification history. We used a surface water bodies dataset derived from the high-resolution maps of global surface water bodies and their long-term changes, with the data span from 16 March 1984 to 31 December 2020. Each pixel was individually classified into water/non-water using an expert system and the results were collated into a monthly history for the entire time period and two epochs (1984–1999, 2000–2020) for change detection. This dataset was generated using 4,453,989 scenes acquired by Landsat 5, 7, and 8, which could better reflect the spatial distribution of surface water bodies (resolution: 30 m) [38]. This yearly seasonality classification collection contains a year-by-year classification of the seasonality of water based on the occurrence values detected throughout the year (acquired in 2020).

(3) Google Earth images. The built-in historical high-resolution image data from Google Earth features a high spatial resolution (maximum resolution up to 0.25 m) and favorable ground–object identification and resolving effects (acquired on 13 July 2020). In addition to the field survey, the spatial distribution of coastal aquaculture ponds was verified using Google Earth high-resolution image data, and verification data points of aquaculture ponds were established on this basis.

(4) Sentinel-2 images. Sentinel-2 images have 12 bands, and different band combinations can be used to classify various ground objects and land cover types. We used the Sentinel-2 median image of the study area from April to August 2020 from the GEE platform, which we used in the post-processing and error elimination of the classification of aquaculture ponds.

(5) River, lake, and reservoir data. The data of regional rivers, lakes, and reservoirs came from OpenStreetMap (https://www.openstreetmap accessed on 31 August 2022). Then, the needed water surface data were screened from the point–line–surface data acquired on this platform (acquired on 20 December 2020), and the coordinate system of this dataset was identical with that of the remote sensing image (WGS-1984).

(6) Land cover data. The LC data for 2020 included three different types of data sources: GlobeLand30 (GLC), ESA-WorldCover (ESA), China Land Cover Dataset (CLCD). GLC is the first global geographic information public product provided by China to the United Nations, and includes data for 2000, 2010, and 2020. GLC uses multi-period Landsat TM/ETM+/OLI, HJ-1 and GF-1 images, with a data accuracy of >86% and data resolution of 30 m (http://www.globallandcover.com accessed on 31 August 2022). ESA provide a new baseline global land cover product at a 10 m resolution for 2020 based on Sentinel-1 and -2 data that was developed and validated in near-real time. The overall accuracy of ESA is 74.4% (https://esa-worldcover.org/en accessed on 31 August 2022). CLCD was released by Yang and Huang [25] at Wuhan University, China. This dataset was based on 335,709-scene Landsat data in GEE, with an overall accuracy of 80% and a spatial resolution of 30 m (https://zenodo.org/record/5816591). The three types of LC data in the study area are displayed in Figure A1.

(6) Other data. The other data included China's administrative boundary data in 2020 and the China Fisheries Statistical Yearbook (acquired in 2020) [37].

2.3. Methods

As shown in the Figure 3, the overall extraction process (Figure 3) of coastal aquaculture ponds in China mainly included: (1) data acquisition and preprocessing; (2) extraction of potential aquaculture ponds; (3) the refined classification of aquaculture ponds; and (4) the evaluation of mapping accuracy. In general, aquaculture ponds are shallow waters, which cannot be effectively distinguished from water bodies such as surface rivers, lakes, reservoirs, and pit-ponds in remote sensing images, so refined processing was performed using the preliminary extraction of potential aquaculture ponds to acquire real surface aquaculture ponds.

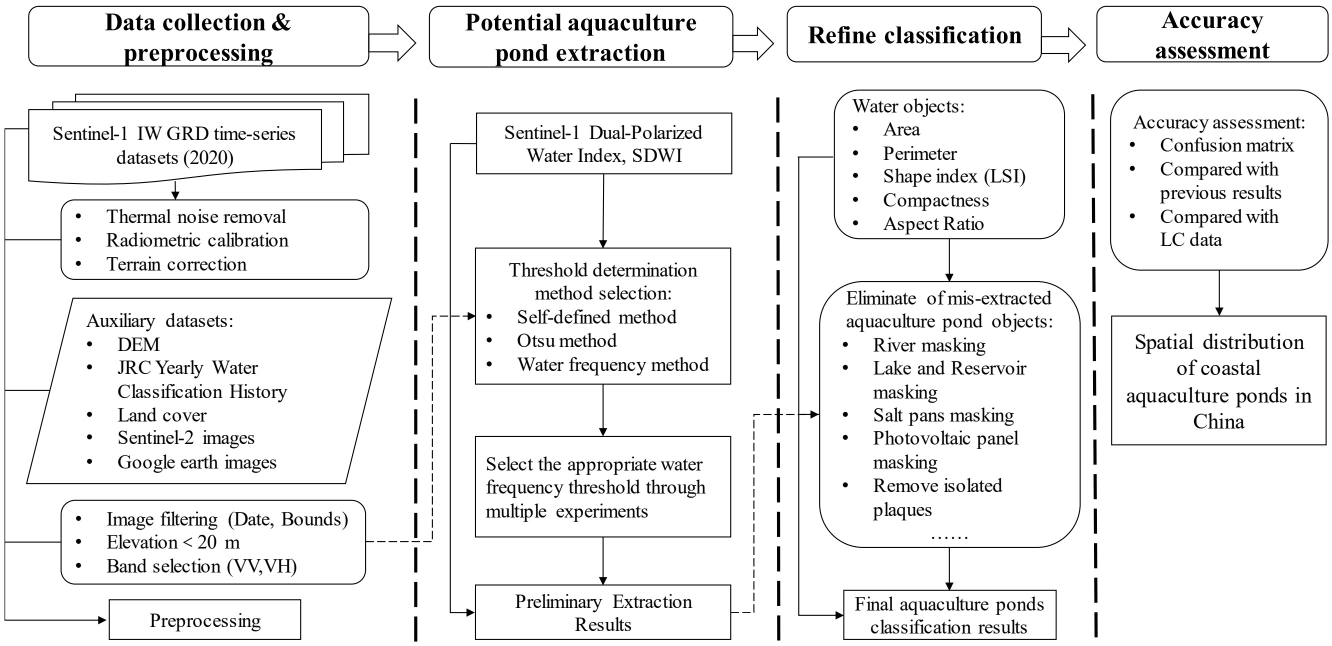

Figure 3. Extraction process from aquaculture ponds.

2.3.1. Preliminary Extraction of Potential Aquaculture Ponds

The selection of a water index is of crucial importance to the extraction of aquaculture ponds. Here, we identified surface water bodies mainly using the Sentinel-1 Dual-Polarized Water Index (SDWI) [39]. Dedicated to Sentinel-1 dual-polarized bands, this index can effectively distinguish the difference between water and other objects in dual-polarized wavebands and can enhance the information of surface water bodies and eliminate disturbances from other surface types such as vegetation and soil. SDWI (Equation (1)) is calculated as:

$$SDWI = \ln(10 \times VV \times VH) - 8 \quad (1)$$

where VV and VH denote the pixel values of the VV median image and VH median image, respectively.

Using the water index, we compared the three methods of self-defined, OTSU, and water frequency to determine the appropriate threshold for segmentation. The aquaculture ponds in coastal plains of Jiangsu were used as a test case (Figure 4a). First, we evaluated the self-defined threshold. Given the significant difference in SDWI between surface water bodies and other ground objects (Figure 4b), the valley (SDWI = -4.438) between two peak values in the SDWI histogram served as the segmentation threshold to separate surface water bodies from other ground objects (Figure 4c). The pixels were classified as water bodies when SDWI was greater than -4.438. Second, we used the OTSU method to divide an image into background and foreground, namely water bodies and non-water bodies, where a greater between-class variance indicated a greater gap between ground objects [40]. So, we found that the OTSU algorithm could be applied to SAR images with an evident peak and valley in the pixel histogram. Third, we evaluated water frequency using a stratified random sampling of regional water body data using the permanent surface water dataset (JRC) to generate random water body samples. We calculated the confidence interval of most water bodies by deducting the doubled variance from the mean value of sampling points and thereby determined the threshold of surface water bodies. The sample points generated by permanent surface water bodies were relatively stable, being basically unchanged within the year, so it could be applied to the SDWI of the Sentinel-1 SAR data. Moreover, sampling all images from April to October and counting the frequency of water bodies could reduce the impact of regional precipitation on SAR images.

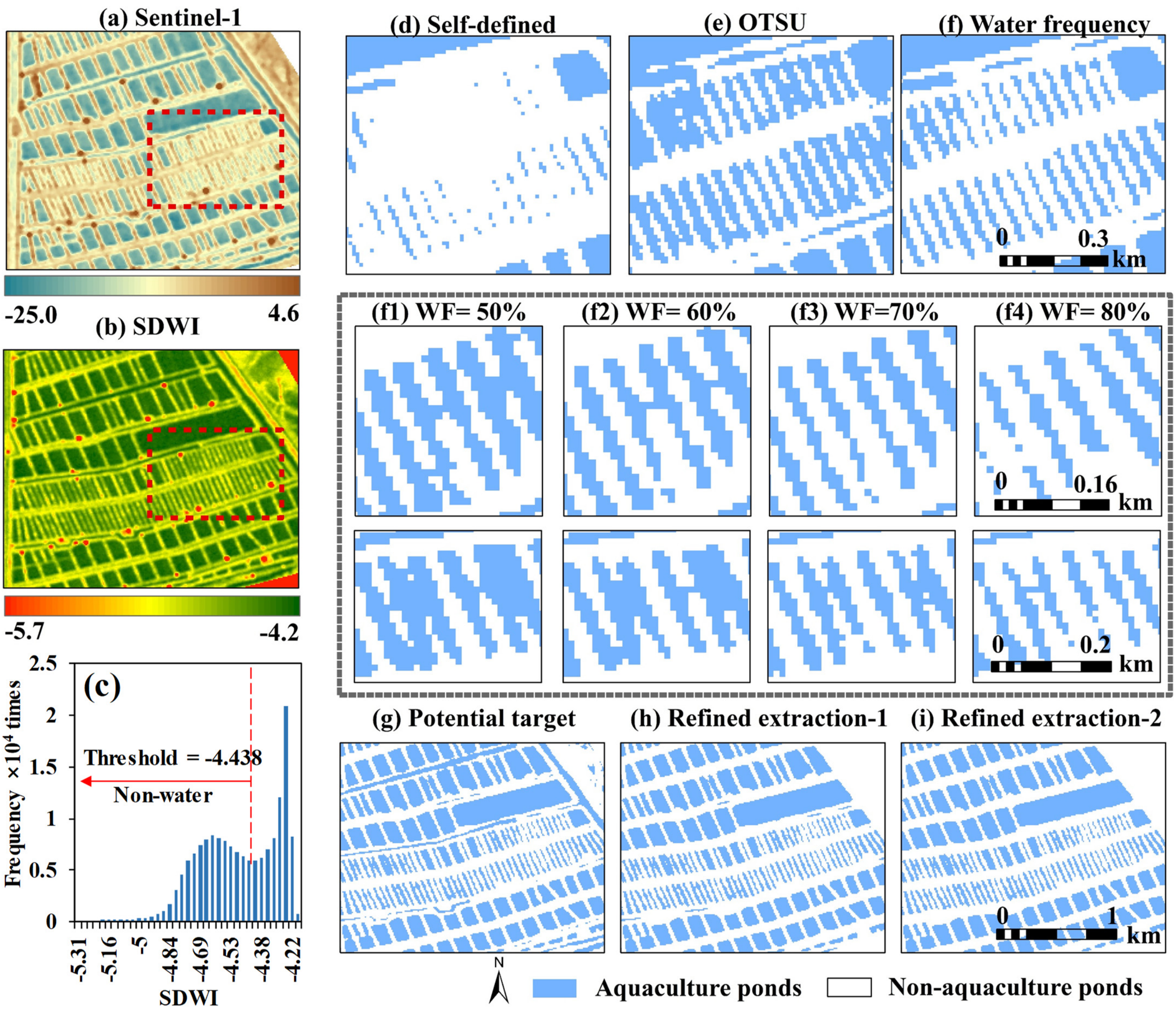

Figure 4. The workflow of aquaculture pond extraction. (**a**) Sentinel-1 original remote sensing image; (**b**) SDWI index; (**c**) frequency distribution of SDWI; (**d**–**f**) identification effect of potential aquaculture ponds after determining thresholds for self-defined, OTSU, and water frequency (WF) methods; (**f1**–**f4**) potential aquaculture pond identification effects under different water frequencies; (**g**) potential aquaculture pond targets; (**h**) object feature extraction of aquaculture ponds; and (**i**) elimination of other water bodies.

We found the self-defined water body threshold to be less effective (Figure 4d), and this method missed the main water body signal. The OTSU and water frequency methods better identified surface water bodies, but the OTSU method tended to over-identify surface water (Figure 4e). The water frequency method determined the threshold based on permanent surface water bodies. During April–October, the coastal aquaculture ponds in China remain shallow and are relatively stable, so the water frequency method was more reliable and practical during this period (Figure 4f). The key to determine the threshold value according to the water frequency method is the frequency, so here we experimented with a water frequency of 50–80% for the same region and found that, with a water frequency of <60% (Figure 4f1,f2), a wide range of aquaculture ponds were identified and had a poor segmentation effect. When the water frequency was >70% (Figure 4f4), partial water body information was easily excluded. We found that when water frequency was between 60% to

70% (Figure 4f3), the water bodies were effectively segmented, and most of the information of surface water bodies was preserved.

2.3.2. Refined Classification of Aquaculture Ponds

(1) Object feature extraction of aquaculture ponds

Since 2015, the standardization transformation of aquaculture ponds has been rapidly promoted by coastal aquaculture studies, namely, the pond shape, pond area, and ridge width. Hence, the object features of potential aquaculture ponds were extracted in this study using the area, perimeter, aspect ratio(AR) (Equation (2)), shape index (LSI) (Equation (3)), and compactness (Equation (4)) of aquaculture ponds based on the relatively regular morphological characteristics of coastal aquaculture ponds [16,41]. The calculation formula is as follows:

$$Aspect\ Ratio = \frac{Width}{Height} \tag{2}$$

$$LSI = \frac{Perimeter \times 0.25}{\sqrt{Area}} \tag{3}$$

$$\text{Compactness} = \frac{Width \times Height}{Area} \tag{4}$$

where Width, Height, Perimeter, and Area stand for the width, length, perimeter, and area of plaques, respectively.

As shown in Figure 4g, we excluded the ponds that were too small (<0.01 km^2) or too large (>10 km^2) and those with short perimeters (<150 m) were excluded. We found through repeated experiments that for all aquaculture ponds in the experimental area, the AR, LSI, and Compactness were always greater than 1.11, 1.2, and 0.3, respectively. The irregularly shaped water surface bodies (Figure 4h) with unreasonable areas and perimeters could be effectively eliminated through object feature extraction.

(2) Elimination of other water bodies

The aquaculture pond data acquired in the previous step were masked using surface water bodies, including rivers, lakes, and reservoirs, provided by OpenStreetMap. Using high-resolution images from Google Earth and 10 m remote sensing images from Sentinel-2, obvious non-aquaculture ponds (channels, streams, and saltpans) or isolated water bodies were removed to obtain a more accurate map of coastal aquaculture ponds. It could be observed from Figure 4i that isolated plaques and aquaculture-pond-like channels dedicated for water drainage or diversion could be effectively eliminated through post-classification using high-resolution images.

2.3.3. Accuracy Verification

To assess the accuracy of coastal aquaculture ponds in China, a total of 9155 random points were generated in the study area, including 2555 non-aquaculture pond sample points and 6600 aquaculture pond sample points (Figure 5). The sample points were visually interpreted using high-resolution images from Google Earth in 2020, and an aquaculture pond and non-aquaculture pond confusion matrix was constructed. Finally, the extraction accuracy was evaluated by calculating the overall accuracy (OA) and Kappa coefficients of the confusion matrix. Using the verification sample sets of aquaculture ponds and non-aquaculture ponds in the study area, we calculated the user's accuracy (UA), producer's accuracy (PA), and OA for aquaculture ponds and non-aquaculture ponds.

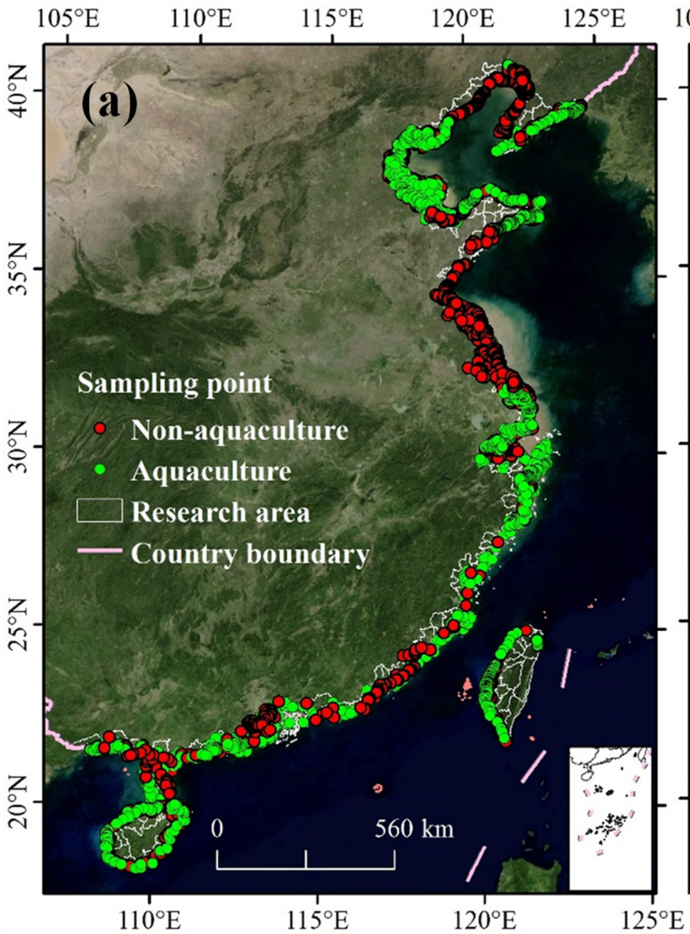

Figure 5. Spatial distribution of (**a**) sampling points and (**b**) verification points.

Furthermore, it was necessary to strengthen the comparison between the study results and other LC data products in order to characterize the identification effect on coastal aquaculture ponds—a concrete type of LC. Three main LC products were selected, GLC, ESA, and CLCD, and we performed spatial overlay analysis on the identification results of aquaculture ponds and the three types of LC data. We counted the aquaculture pond area and water areas in different provinces, cities, and counties, and the correlation coefficient was used to characterize the relationship between the two. These correlations also reflected the credibility of the research results to a certain extent.

2.3.4. Nuclear Density Analysis

As a common method for hot-spot analysis of geographic elements, the nuclear density analysis method can better reflect the spatial agglomeration and distribution characteristics of a geographic element. The nuclear density analysis (Equation (5)) was calculated as:

$$f_h(x) = \frac{1}{nh}\sum_{i=1}^{n} k(\frac{x - x_i}{h}) \quad (5)$$

where $f_h(x)$ is the nuclear density function; n is the sample point; h is the bandwidth, that is, the search radius; K is the nuclear function; and $x - x_i$ is the distance from the predicted value x to the sample x_i. The nuclear density analysis of aquaculture ponds was performed using the ArcGIS10.5 spatial analysis module.

3. Results

3.1. Accuracy Assessment

The OA was 93% and the Kappa coefficient was 0.84 (Table 1), which indicated that our aquaculture pond classification methods had high accuracy. From a provincial level (Figure A2), the OA and Kappa coefficients were the highest in northern Liaoning, Hebei, Tianjin, and Shandong, whose overall accuracy and Kappa coefficients were approximately 1. In Zhejiang and Fujian Provinces, the OA and Kappa coefficients were low, where the OA was 0.88 and the Kappa coefficient was 0.78, which was mainly ascribed to the irregular shapes and small aquaculture pond areas in these provinces and a lower identification effect than with the northern large-scale aquaculture ponds. In southern Hainan and Taiwan, the OA and Kappa coefficients were high, with an overall accuracy of 0.96 and 0.91, respectively. The UA was lower than 0.90 only in Fujian (0.86) and Guangxi (0.87) and was greater than 0.90 in the other provinces. The PA was low in Fujian (0.87) and Guangdong (0.87) and greater than 0.90 in other provinces.

Table 1. Confusion matrix of extraction results and manual interpretation results.

Types	Non-Aquaculture	Aquaculture	Sum
Non-aquaculture	2264	315	2579
Aquaculture	291	6285	6576
Sum	2555	6600	9155
User's accuracy (UA)	0.88	0.96	
Producer's accuracy (PA)	0.89	0.95	
Overall accuracy (OA)	0.93		
Kappa	0.84		

3.2. Spatial Distribution of Coastal Aquaculture Ponds

All aquaculture ponds (>0.005 km^2, totaling 6937 km^2) in the coastal county-level cities of China were extracted. At the provincial level (Figure 6a), the densities of coastal aquaculture ponds were the largest in Shandong, Guangdong, and Jiangsu, and were 1557, 1032, and 1028 km^2, respectively, which accounted for 22.49%, 14.90%, and 14.84% of the total aquaculture pond area in the study area. In addition, the area ratio of aquaculture ponds was greater than 10% in both Liaoning (LN) and Hebei (HB), and was small in Fujian (FJ) (5.51%), Tianjin (TJ) (4.73%), Zhejiang (ZJ) (4.51%), Taiwan (TW) (3.52%), Guangxi (GX) (2.52%), and Hainan (HN) (1.00%), and was smallest in Shanghai (SH), Hong Kong (MK), and Macao (M).

At the prefecture city level (Figure 6b), we selected and displayed only the administrative units that ranked in the top 27 (area ratio > 1%) in the aquaculture pond area. Among all the coastal prefecture-level cities, the aquaculture pond area was the largest in Yancheng City (YC), with an area ratio of 10.59%, which was much higher than that in other coastal prefecture-level cities. Thus, there was intense aquaculture production activity in this city, where the straight coastline and rich silted mudflat resources provided superior conditions for the development of aquaculture ponds, and coastal land reclamation activities ensured abundant land resources so that large-area and regularly shaped coastal aquaculture ponds are distributed in Yancheng City. Secondly, the area ratios of aquaculture ponds in Dongying (DY), Binzhou (BZ), Tangshan (TS), and Dalian (DL) were 9.72%, 8.51%, 8.03%, and 6.79%, respectively. All of the aforementioned prefecture-level cities are distributed near Bohai Bay, where the alluviation effect of sea waves is weakened, which contributes to the dense distribution of large-scale aquaculture ponds. The area ratios of aquaculture ponds in Tianjin (TJ) (4.73%), Cangzhou (CZ) (3.40%), Lianyungang (LYG) (2.89%), Jiangmen (JM) (2.87%), Zhanjiang (ZJ) (2.43%), Jinzhou (JZ) (2.25%), and Fuzhou (FZ) (2.00%) were all greater than 2%, while the aquaculture pond area in other prefecture-level cities was relatively small.

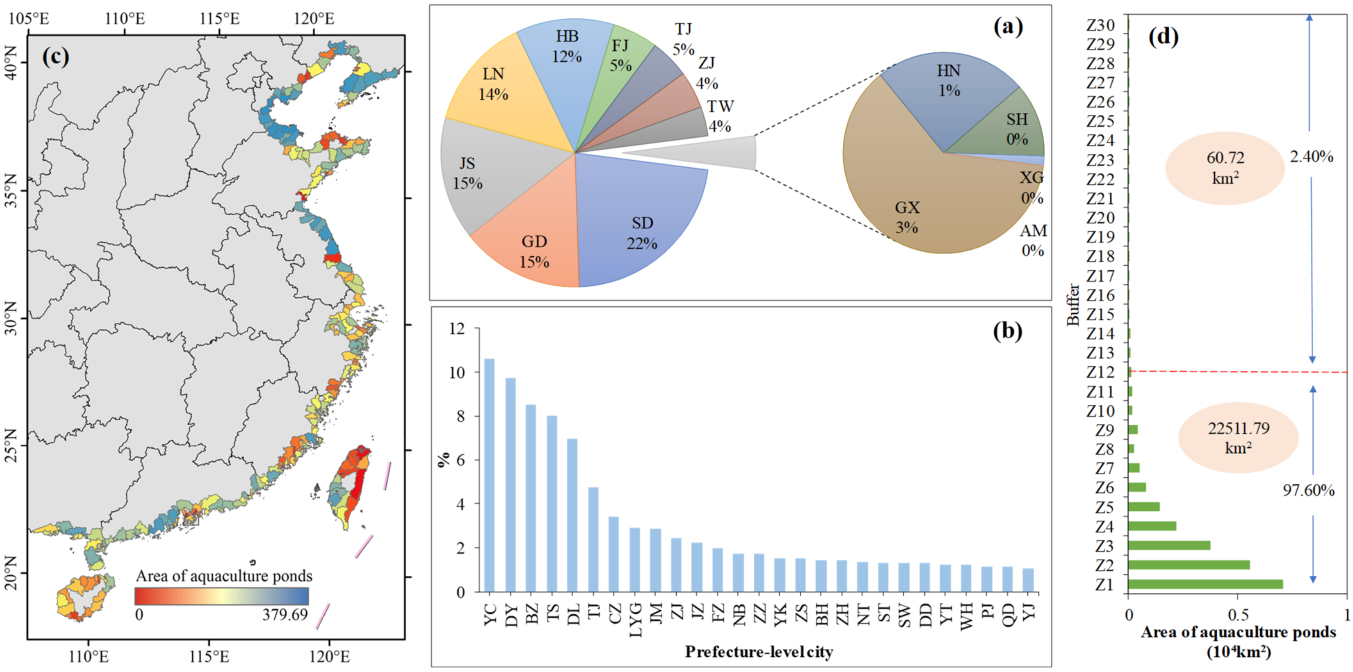

Figure 6. Area distribution of aquaculture ponds along the coast of China. (**a**) The area distribution of aquaculture ponds in each province; (**b**) the distribution of the top 27 prefecture-level cities in terms of aquaculture pond area; (**c**) aquaculture pond area at the city level; (**d**) west coast of Taiwan Province as an example of the number of aquaculture pond areas in 30 buffer zones.

At the county scale (Figure 6c), the high-value areas of aquaculture ponds were consistent with those at the prefecture city level and were concentrated in Shandong, Tianjin, and Hebei Provinces on the west side of the Bohai Gulf. The top five counties in terms of aquaculture pond area were Hekou District (Dongying City), Caofeidian District (Tangshan City), Binhai New District (Tianjin City), Wudi County (Binzhou City), and Zhanhua District (Binzhou City). The aquaculture pond area in counties on the north side of Jiangsu Province was also large, and aquaculture ponds were densely distributed near the seaside. In south China, the aquaculture pond area was large only in Taishan City, Zhongshan City, and in the Xinhui District of Guangdong Province; Fuqing City and Zhangpu County in Fujian Province; Hepu County in Guangxi Province; and Zhangpu County in Taiwan. Thus, the aquaculture pond area in north China was much larger than in south China.

From the perspective of land and sea distribution, given the large south–north span of coastal zones in China, a total of 30 buffer zones were generated along the west coastal zone in Taiwan (Figure 6d), whose areas of aquaculture ponds were calculated. We discovered that 97.63% of the aquaculture ponds were concentrated in the coastal zones within 120 km along the coastline, and only 2.37% of the aquaculture ponds were distributed in inland areas beyond 120 km along the coastline, which indicated that aquaculture ponds were highly concentrated along the seaside areas. Seaside aquaculture ponds were denser and larger due to the abundant seaside land resources, which made it convenient for constructing large-scale aquaculture ponds. Inland aquaculture ponds were scattered near rivers, lakes, and reservoirs. Considering the shortage of land resources for aquaculture inland, the inland aquaculture pond area was generally small.

Aquaculture ponds were concentrated near coastal estuary deltas, coastal plains, and gulfs (Figure 7a). The longitudinal distribution (Figure 7b) of aquaculture ponds was dense within the region 117.42°E–118.81°E, which is located at the border between Hebei and Shandong and the west side of the Bohai Gulf. In addition, the area of such aquaculture ponds was larger than in south China. In terms of latitudinal distribution, there were three dense aquaculture pond areas (Figure 7c) in the Pearl River Delta (21.29°N–24.22°N) in Guangdong Province, the coastal plains (32.27°N–34.67°N) in Yancheng City, Jiangsu Province, and the coastal plains (37.38°N–40.92°N) in the northern Yellow River Delta.

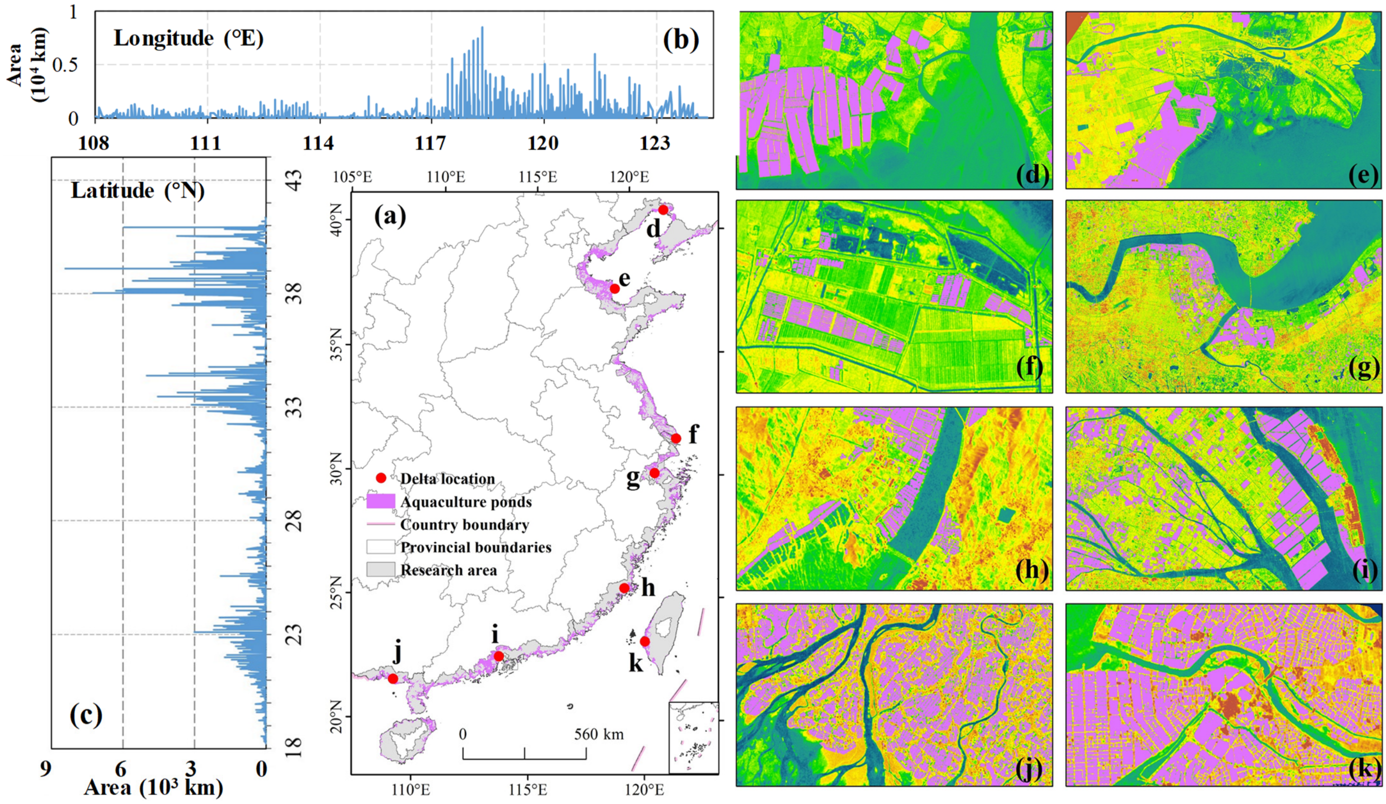

Figure 7. Spatial distribution characteristics of aquaculture ponds along the coast of China. (**a**) The spatial distribution of aquaculture ponds; (**b**) the aquaculture pond area at 0.1° longitude; (**c**) the aquaculture pond area at 0.1° latitude; (**d**–**k**) superimposed images of the eight estuary delta Sentinel-1 images and aquaculture ponds, in which (**d**) is the Liaohe delta (121° 47′41″E, 40° 54′23″N); (**e**) is the Yellow River delta (119° 4′39″E, 37° 45′40″N); (**f**) is the Yangtze Estuary delta (121° 35′53″E, 31° 33′36″N); (**g**) is the Qiantang River Delta (120° 46′50″E, 30° 11′15″N); (**h**) is the mouth of Xinghua Bay in Fujian (119° 15′23″E, 25° 28′57″N); (**i**) is the Pearl River Delta (113° 39′48″E, 22° 41′28″N); (**j**) is the Nanliujiang Delta in Guangxi (109° 3′5″E, 21° 36′58″N); and (**k**) is the Jishuixi Delta in Taiwan (120° 7′40.15″E, 23° 17′35″N).

We chose and displayed eight of the largest coastal estuary deltas and gulfs in China. Figure 7d shows the Liao River Delta plain in Liaoning Province, where a large area of aquaculture ponds was concentrated on the west side of the estuary. These aquaculture ponds were large, regularly shaped, and dense. Figure 7e exhibits the Yellow River Delta, where aquaculture ponds were concentrated in the south of the estuary and densely distributed in seaside areas, with a large area and a regular shape. Figure 7f shows Chongming Island in the Yangtze Estuary Delta, where the distribution of coastal aquaculture ponds was small since this area is close to the socioeconomically developed Shanghai. Figure 7g displays the Qiantang River estuary, where the south side of the river is rich in land resources that have accumulated silt and have a dense distribution of small-scale aquaculture ponds. Figure 7h displays the Xinghua Bay in Fujian Province, where aquaculture ponds were densely distributed along the two sides of the port. Figure 7i shows the Pearl River Delta in Guangdong Province, which had small-scale aquaculture ponds that were irregularly shaped, densely distributed, and covered a wide area. Figure 7j exhibits the Nanliu River Delta in Guangxi Province, where small, irregularly-shaped aquaculture ponds were spread all over the delta plain, which has an advantageous geographical location for aquaculture pond construction. Figure 7k shows the Driving Creek Delta plain in Taiwan, where the terrain is flat on both sides and had a dense distribution of small-scale aquaculture ponds.

From the perspective of spatial agglomeration, the coastal aquaculture ponds in China showed significant spatial agglomeration characteristics (Figure 8), but the spatial heterogeneity was also prominent, with the nuclear density ranging from 0 to 13.35. The high-nuclear-density areas were concentrated in coastal areas such as estuary deltas, gulfs, and coastal plains, among which 12 obvious high-nuclear-density values were chosen. Areas 1, 2, 4, 11, and 12 were coastal plains; areas 5, 6, 7, and 8 were gulfs; areas 3, 9, and 10 represented estuaries and estuary deltas. Areas 3, 9, and 8 represented the Yellow River Delta, the Pearl River Delta, and the estuary of Chindwin River and Dalan River in Guangxi Province, respectively. In the above three areas, the terrain was flat with densely distributed river networks, and aquaculture ponds were densely distributed near estuaries.

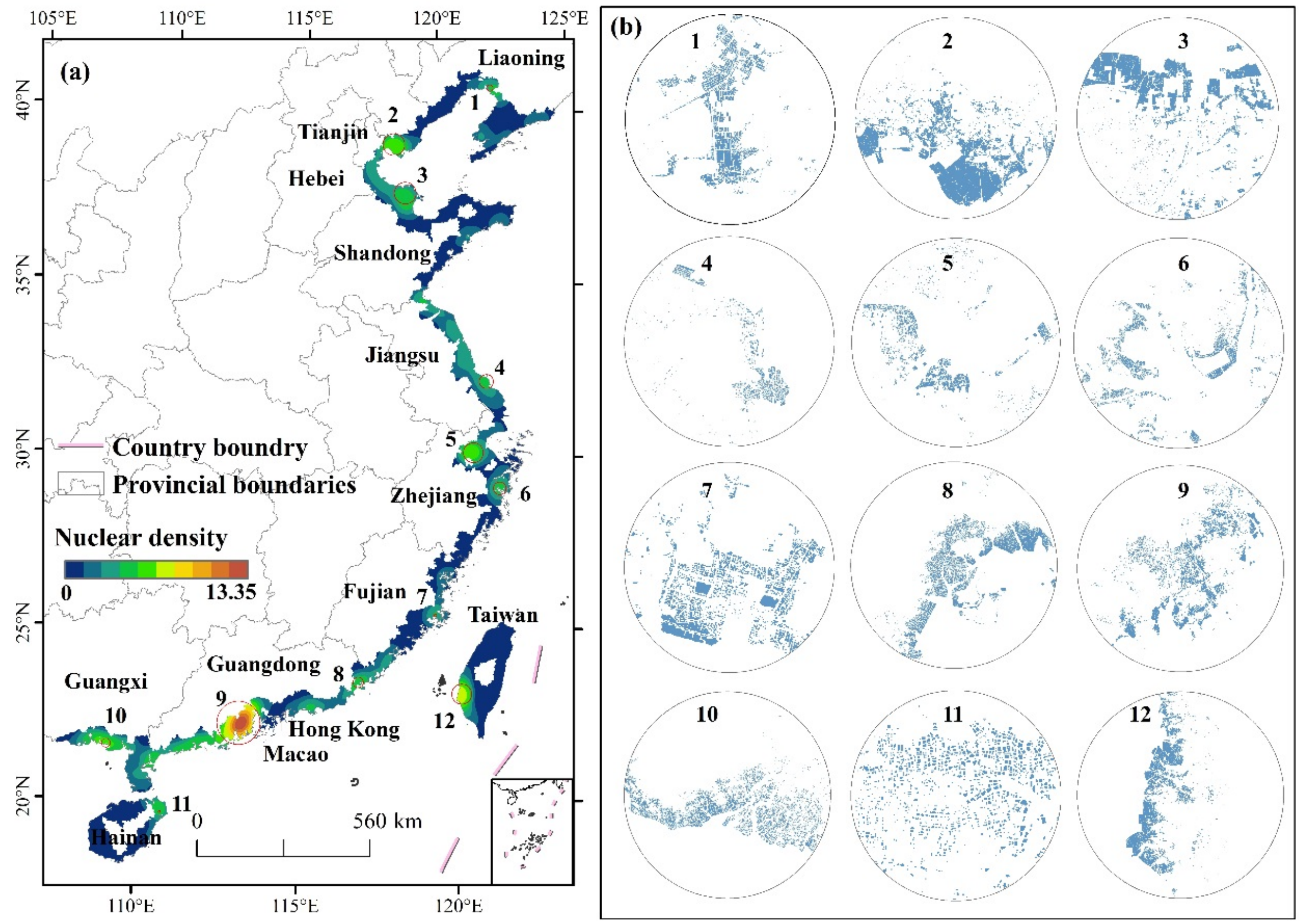

Figure 8. Spatial agglomeration characteristics of aquaculture ponds along the coast of China. (**a**) Characteristics of nuclear density distribution in aquaculture ponds; and (**b**) distribution characteristics of aquaculture ponds in areas with high nuclear density.

3.3. Comparison between Aquaculture Ponds and Different Land Cover Products

As shown in Figure 9, the extracted aquaculture ponds were compared with the three types of LC products. First, the overlapping area between our extracted aquaculture ponds and GLC data was 5363 km^2, or 77.31%, which indicated that the spatial distribution of the aquaculture ponds we identified agreed well with the GLC data products and reflected that our resultant maps were a highly reliable. The spatial resolution of GLC products was 30 m, so the plaques of this type of product were large, and the water areas had a wide-range distribution characteristic (Figure 9c,g,k,o,s). Second, the overlapping area between our aquaculture pond map and the ESA data products was 73.98%. The resolution of the ESA products was 10 m, which matched the resolution of our aquaculture pond map. As shown in Figure 9d,h,l,p,t, these products had a high accuracy, and the ground object distribution was basically consistent with aquaculture ponds. Finally, the overlapping area between our aquaculture pond map and CLCD was 61.81%. Except for Figure 9e, the spatial distribution of water areas in other selected areas was basically identical with the aquaculture ponds, and the resolution of the CLCD data products was 30 m, but the mapping plaques were evidently smaller than those of the GLC data (Figure 9i,m,q,u).

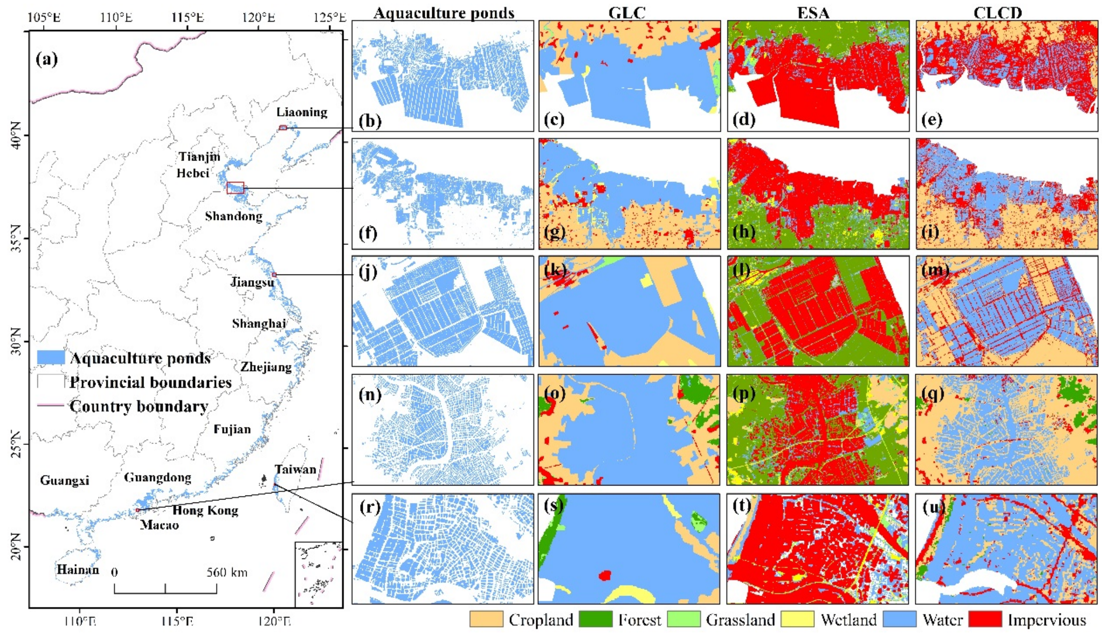

Figure 9. Comparison of our aquaculture ponds with three land cover products. (**a**) Spatial distribution of aquaculture ponds; (**b**,**f**,**j**,**n**,**r**) distribution of aquaculture ponds in typical areas; and (**c**–**e**,**g**–**i**,**k**–**m**,**o**–**q**,**s**–**u**) superimposed features of aquaculture ponds and three land cover products.

At the provincial level, the areas of aquaculture ponds in all provinces were smaller than the water area in the three LC products and had identical distribution characteristics with the areas of the three types of water areas, namely, the water area and aquaculture ponds were the largest in Guangdong, Jiangsu, Liaoning, and Hebei (Figure 10a). In addition, the aquaculture pond area in the different provinces that we identified in this study was highly correlated with the three LC data products ($R^2 > 0.90$), among which the aquaculture pond area had the highest correlation with the ESA products ($R^2 = 0.96$), which indicated that the 10-meter ESA data products had a favorable ground object identification effect (Figure 10b).

At the prefecture-city level, aquaculture pond areas and LC products in 63 prefecture-level cities were extracted as shown in Figure 10c. We found that aquaculture ponds in prefecture-level cities had the highest correlation with the ESA products ($R^2 = 0.84$), followed by the GLC ($R^2 = 0.83$) and CLCD data products ($R^2 = 0.77$). In addition, the aquaculture pond area in different prefecture-level cities tended to be smaller than that of the three types of LC data products (9d). The water area of the GLC data products was the largest, followed by the ESA and CLCD data products. In the prefecture-level cities, the aquaculture pond area was the largest in Yancheng, Dongying, Binzhou, Tangshan, and Dalian. In the CLCD products, the aquaculture pond area was the largest in Shanghai, Dongying, Yancheng, Binzhou, and Tangshan. For the ESA products, the aquaculture pond area was the largest in Dongying, Shanghai, Binzhou, Dalian, and Yancheng. In the GLC products, the aquaculture pond area was the largest in Dongying, Yancheng, Shanghai, Binzhou, and Dalian.

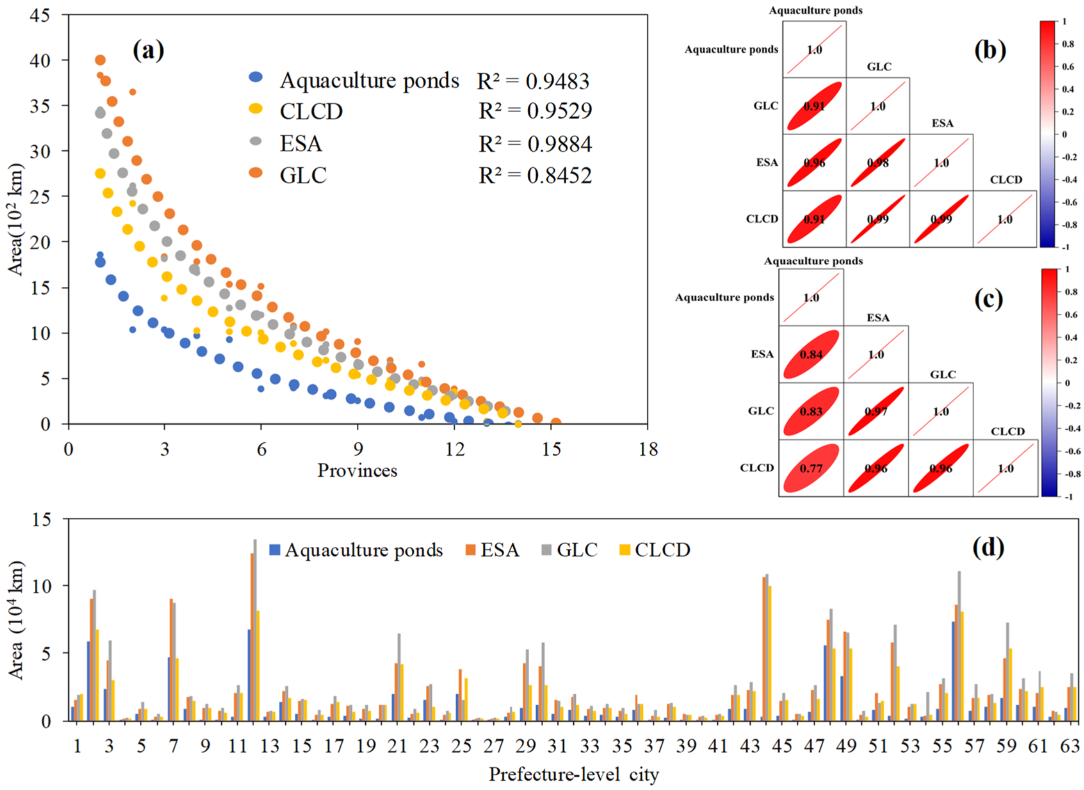

Figure 10. Statistics on the correlation between the aquaculture pond area and the water area of three land cover products in different provinces, cities, and counties. (**a**) Distribution of aquaculture ponds and water areas in provinces; (**b**,**c**) correlations between aquaculture ponds and water areas in provinces and prefecture-level cities; and (**d**) distribution characteristics of aquaculture ponds and water areas in prefecture-level cities.

4. Discussion

4.1. Uncertainties Resulting from Methods and Data

Our classification framework had a good classification effect by virtue of GEE cloud processing and ArcGIS software. As for the comparisons of the data results, our extracted area was basically identical with the actual situation in all the provinces, with the correlation coefficient reaching as high as 86.69%. At the provincial level, the area of extracted coastal aquaculture ponds in Guangxi Province (174.36 km^2) was basically consistent with the classified aquaculture pond area in Beibu Gulf in Guangxi Province (199.3 km^2) [42], and that (1031.72 km^2) in Guangdong Province basically agreed with the study results (1369.00 km^2) of Huang and Wei [41].

Using radar backscattering images (Sentinel-1 SAR data), our method captured the water surface roughness using SDWI and effectively identified all aquaculture ponds in the study area by combining the water frequency. However, the attenuation of the backscattering cross section of SAR images by rainfall cannot be ignored. Therefore, we performed a statistical analysis on the SDWI index of all the images in the study area to comprehensively consider the response of all the SAR images to water body signals. Moreover, paddy fields and aquaculture ponds could be effectively distinguished through time-based screening (April–October); other water bodies such as rivers, lakes, reservoirs, and wetlands could be effectively distinguished through the relatively spatial geometric object features of aquaculture ponds. Sources of error such as saltpans, photovoltaic panels, and waste ponds were eliminated through visual interpretation. Based on previous studies, therefore, our method improved the mapping of coastal aquaculture ponds and could be applied for the mapping of aquaculture ponds in other areas.

Of course, different scholars have adopted different data sources and methods to classify coastal aquaculture ponds, which leads to differences among the study results. In our study, the aquaculture pond area we extracted in coastal county-level cities in China was 6938 km^2, which was larger than the area of 3761 km^2 reported in the 2020 China Fisheries Statistical Yearbook, mainly because some inland freshwater aquaculture ponds existed in our study area. In addition, our results were slightly lower than the results of the aquaculture ponds extracted by Duan et al. [18] (9614 km^2) in coastal 30 km buffer zones of China in 2020. This difference was mainly because Duan et al. [18] used Landsat images (resolution: 30 m) and the area of the extracted aquaculture ponds was large, while the aquaculture pond area extracted using Sentinel-1 images (resolution: 10 m) was closer to the real area of aquaculture ponds. Moreover, the 30 km buffer zones differed, to some extent, from coastal county-level cities in this study, which led to differences in the results between the two. Hence, several uncertainties should be considered when applying the proposed method to other areas.

First, as for the selection of data sources, Landsat images are suitable for exploring the long-time-series spatial–temporal variation characteristics of aquaculture ponds, while the Sentinel data can realize the refined mapping of aquaculture ponds within a short time series since 2014. Second, the waterlogging frequency of aquaculture ponds varies from area to area, so the monthly series data every year should be selected according to the precipitation and aquaculture ponds in the study area. For instance, Sun et al. [16] extracted the January-April Sentinel-1 SAR data in 2020 for the classification of regional aquaculture ponds in Vietnam. Stiller et al. [26] selected all the Landsat images from September 2014 to September 2016 for classifying aquaculture ponds in the Yellow River Delta and Pearl River Delta in China. Finally, the information of water bodies with high inundation frequencies, such as saltpans, reservoirs, and tidal flat wetlands, exists in different areas, so the classification is inseparable from later-stage manually refined processing.

4.2. Sources of Errors in Aquaculture Pond Identification

The key to the extraction of coastal aquaculture ponds lies in distinguishing between water and land. Therefore, the SDWI constructed by Sentinel-1 images was selected in our study, which could effectively distinguish water bodies from land. In addition, the images from April to October were selected, which was the growing season of coastal rice, so the SDWI was able to distinguish paddy fields from aquaculture ponds. However, errors were unavoidable in the classification of coastal aquaculture lands, and in particular there was abundant information on coastal water bodies along with water sources in addition to aquaculture ponds. Some surface water bodies, such as rivers, lakes, and reservoirs were masked through OpenStreetMap, but some remaining water bodies were sources of error.

First, salt pans are a special type of industrial and mining land and are artificial water bodies used for salt production. They are distributed in a large continuous area in a regular block shape near the silty coast. Our study period was April–October, the same time frame as salt manufacturing in salt fields, so the salt pans in the study area were filled with seawater, becoming important water sources of surface water bodies. As shown in Figure 11a, minor differences were observed between salt pans and aquaculture ponds in the original Sentinel-1 images, so such salt pans were all identified as surface water bodies. For example, the brightness of salt pans in Sentinel-2 images (waveband combination: R8-G4-B3) was obviously higher than that of aquaculture ponds.

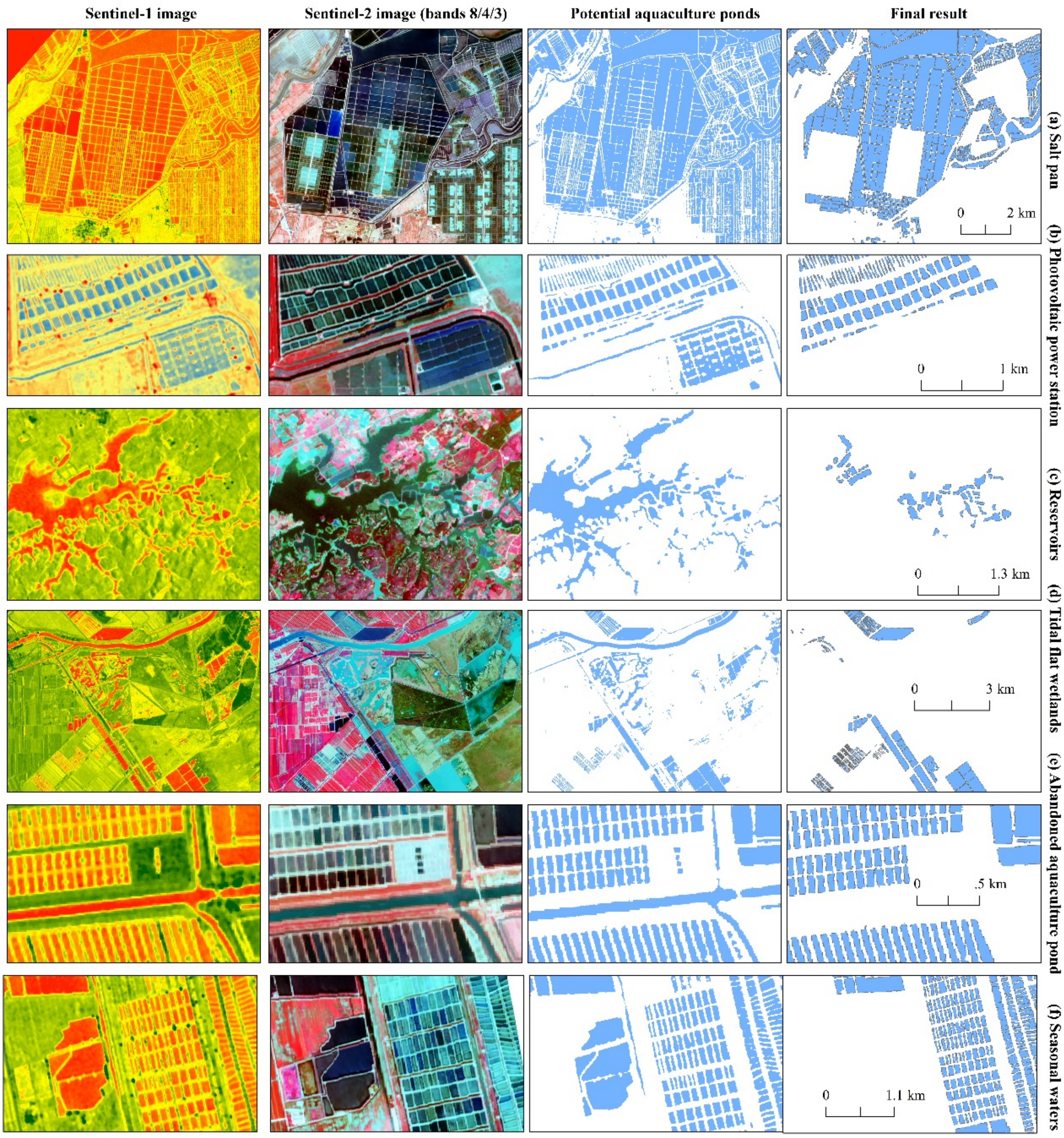

Figure 11. Sources of errors in coastal aquaculture pond extraction. The main error sources in the extraction process of aquaculture ponds were (**a**) salt pans, (**b**) photovoltaic power stations panels, (**c**) reservoirs, (**d**) tidal flat wetlands, (**e**) abandoned fishponds, and (**f**) seasonal water bodies.

Second, coastal areas are rich in land resources and contain rich solar energy resources, so coastal photovoltaic power stations possess excellent resource advantages. Hence, a lot of photovoltaic power stations have been built in coastal areas of China. Given that the main extraction objects were pure aquaculture ponds, multi-attribute photovoltaic power stations were removed. As shown in Figure 11b, the water body information beneath photovoltaic panels in the original images were still effectively identified, and they were also identified as surface water bodies in the identification of potential aquaculture ponds, so they were removed. Third, as shown in Figure 11c, the coastal hilly area of Guangdong Province had aquaculture ponds that were distributed near reservoirs, but some small reservoirs could not be distinguished from aquaculture ponds during classification, which was also an important source of error that influenced our results.

Fourth, although tidal flat wetlands were included in the extraction results of potential aquaculture ponds, some irregular tidal flat wetlands could be removed using object-oriented features (Figure 11d), while some relatively regular tidal flat wetlands could only be determined by combining high-resolution images and visual interpretation. Thus, the extraction results of aquaculture ponds were also influenced, to some extent, by seaside tidal flat wetlands. Fifth, some aquaculture ponds in coastal areas are subjected to serious bottom hardening through multi-year production activities with a high operating cost, so they are idled as abandoned fishponds distributed in all coastal provinces. The inundation frequency of abandoned fishponds was high during April–October, so they could be easily identified as aquaculture ponds (Figure 11e), while this type of ground object had a similar shape to real aquaculture ponds, so they could only be determined by combining high-resolution images and visual interpretation. Finally, the inundation frequency was high in seasonal water bodies that serve as important regional water sources. If regular, some seasonal water bodies could be easily identified as aquaculture ponds (Figure 11f). However, seasonal water bodies were distinguished from aquaculture ponds by combining their object features and their lower concentration degree than aquaculture ponds.

Of course, there were more sources of error than those we listed above, such as uncultivated paddy fields, sewage treatment ponds, abandoned rivers, and artificial pond landscapes. The water body information in different areas is varied and complex, so the classification of aquaculture ponds should be conducted according to the actual situation in the study area.

4.3. Sustainable Management of Aquaculture Ponds and Prospects

China's coastal aquaculture ponds display significant spatial heterogeneity, e.g., large-scale aquaculture ponds are densely distributed in northern Hebei and Shandong and small-scale ponds are densely distributed in southern Fujian, Guangdong, and Guangxi, which leads to certain differences in the sustainable development of different aquaculture ponds. For the medium- and large-scale aquaculture ponds in the north, the efficient output of aquaculture ponds can be achieved by improving the quality of fry and optimizing the breeding species. For the small-scale aquaculture ponds in the south, the government should optimize the spatial layout, promote the construction of standardized ponds, and eliminate substandard ponds that pollute the environment.

Moreover, in our study, we combined the Sentinel-1 SAR data with the water frequency method to efficiently map aquaculture ponds along the coast of China. However, the research time scale was only for 2020. In future research, we can apply this method to long-term aquaculture pond identification to investigate the temporal and spatial variation characteristics of coastal aquaculture ponds. In particular, the intensity of human activities in the coastal zone is increasing rapidly, and the expansion or reduction in aquaculture ponds have a significant impact on the regional ecological environment, which also requires the long-term mapping of aquaculture ponds.

5. Conclusions

Currently, the human demand for food, food diversity, and food nutrition are unprecedentedly high, and we accurately mapped coastal aquaculture ponds to provide information that can be used to optimize the spatial layout of fishery aquaculture activities and ensure fishery food security. Our maps highlight the spatial heterogeneity of aquaculture ponds and provide a basis for decision making by the government to formulate aquaculture-pond-planning policies.

Here, we used aquaculture-pond-mapping methods that were based on GEE cloud processing and ArcGIS local processing. Using Sentinel-1 SAR high-resolution remote sensing images (10 m), our method combined the water index and water frequency to comprehensively identify regional potential aquaculture ponds, and we acquired a relatively refined and accurate dataset of the spatial distribution of aquaculture ponds in the coastal areas of China by combining the regular object features and refined classification. Our main conclusions were:

(1) Our method had a high classification accuracy (the overall accuracy was 0.93), which indicated that our method could be applied to map aquaculture ponds in other areas;

(2) The spatial heterogeneity of coastal aquaculture ponds in China was prominent, and large-scale dense aquaculture ponds played a dominant role in north China while small-scale ponds were dominant in south China;

(3) Our method was highly correlated with other land cover data products, accompanied by a more refined identification of aquaculture pond plaques;

(4) The classification of aquaculture ponds was complicated by sources of error, such as salt pans, photovoltaic panels, reservoirs, tidal flat wetlands, abandoned aquaculture ponds, and seasonal water bodies.

Author Contributions: Conceptualization, P.T., Y.L. and J.L.; methodology, P.T., Y.L. and H.Z.; software, P.T. and H.Z.; writing—original draft preparation, P.T., Y.Y. and Y.L.; writing—review and editing, P.T., Y.L., L.C. and R.P.; supervision, H.Z., S.A. and Y.Y. All authors have read and agreed to the published version of the manuscript.

Funding: This research was funded by National Natural Science Funded project (41976209, 42206236), College Students' Science and Technology Innovation Activity Plan and Xinmiao Talent Plan of Zhejiang Province (2022R405B086), and Postgraduate Research and Innovation Fund of Ningbo University (IF2022021).

Acknowledgments: The authors express their gratitude to the editors and the anonymous reviewers for providing valuable comments and suggestions to improve the paper.

Conflicts of Interest: The authors declare no conflict of interest.

Appendix A

Table A1. Summary of previous studies on extraction from aquaculture ponds.

Years	Region/Local	Country	Multiple Countries
1984–2016	Stiller et al (2019) +	Ren et al (2019) *	
1990,1995, 2000, 2005, 2008,2011, 2014, 2017, 2020		Duan et al (2021) *	
1988–2018	Duan et al (2020) *		
1987–2018	Fu et al (2021) *		
2014–2016			Ottinger et al (2017) #
2014–2017		Prasad et al (2019) #	
2016	Yu et al (2020) #		
2019			Ottinger et al (2021) #
2020		Sun et al (2021) #; Duan et al (2020) *	

* Landsat data were used; # Sentinel data were used; + Landsat and Sentinel data were used.

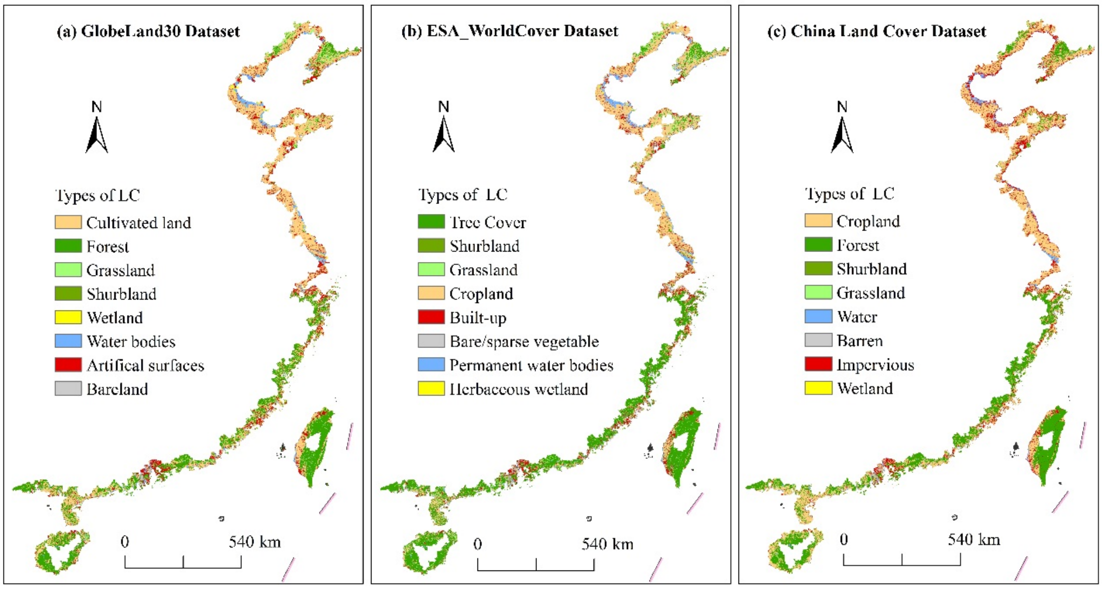

Figure A1. Distribution of three types of land cover data products in the study area.

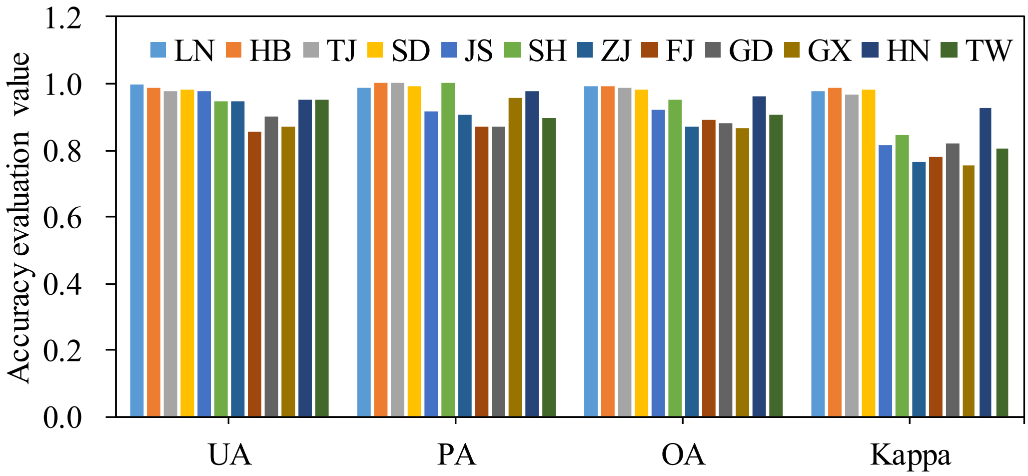

Figure A2. Extraction accuracy of aquaculture ponds in different provinces.

References

1. Cole, D.W.; Cole, R.; Gaydos, S.J.; Gray, J.; Hyland, G.; Jacques, M.L.; Powell-Dunford, N.; Sawhney, C.; Au, W.W. Aquaculture: Environmental, toxicological, and health issues. *Int. J. Hyg. Environ. Health* **2009**, *212*, 369–377. [CrossRef]
2. Kobayashi, M.; Msangi, S.; Batka, M.; Vannuccini, S.; Dey, M.M.; Anderson, J.L. Fish to 2030: The Role and Opportunity for Aquaculture. *Aquac. Econ. Manag.* **2015**, *19*, 282–300. [CrossRef]
3. Stentiford, G.D.; Sritunyalucksana, K.; Flegel, T.W.; Williams, B.A.P.; Withyachumnarnkul, B.; Itsathitphaisarn, O.; Bass, D. New Paradigms to Help Solve the Global Aquaculture Disease Crisis. *PLoS Pathog.* **2017**, *13*, e1006160. [CrossRef]
4. Béné, C.; Barange, M.; Subasinghe, R.; Pinstrup-Andersen, P.; Merino, G.; Hemre, G.-I.; Williams, M. Feeding 9 billion by 2050—Putting fish back on the menu. *Food Secur.* **2015**, *7*, 261–274. [CrossRef]
5. Hák, T.; Janoušková, S.; Moldan, B. Sustainable Development Goals: A need for relevant indicators. *Ecol. Indic.* **2016**, *60*, 565–573. [CrossRef]
6. Kumar, G.; Engle, C.; Tucker, C. Factors Driving Aquaculture Technology Adoption. *J. World Aquac. Soc.* **2018**, *49*, 447–476. [CrossRef]
7. Wang, X.; Xiao, X.; Xu, X.; Zou, Z.; Chen, B.; Qin, Y.; Zhang, X.; Dong, J.; Liu, D.; Pan, L.; et al. Rebound in China's coastal wetlands following conservation and restoration. *Nat. Sustain.* **2021**, *4*, 1076–1083. [CrossRef]
8. Tian, P.; Li, J.; Cao, L.; Pu, R.; Gong, H.; Liu, Y.; Zhang, H.; Chen, H. Impacts of reclamation derived land use changes on ecosystem services in a typical gulf of eastern China: A case study of Hangzhou bay. *Ecol. Indic.* **2021**, *132*, 108259. [CrossRef]
9. Zhang, X.; Zhang, Y.; Zhang, Q.; Liu, P.; Guo, R.; Jin, S.; Liu, J.; Chen, L.; Ma, Z.; Liu, Y. Evaluation and Analysis of Water Quality of Marine Aquaculture Area. *Int. J. Environ. Res. Public Health* **2020**, *17*, 1446. [CrossRef]

10. Ren, C.; Wang, Z.; Zhang, Y.; Zhang, B.; Chen, L.; Xi, Y.; Xiao, X.; Doughty, R.B.; Liu, M.; Jia, M.; et al. Rapid expansion of coastal aquaculture ponds in China from Landsat observations during 1984–2016. *Int. J. Appl. Earth Obs. Geoinf.* **2019**, *82*, 101902. [CrossRef]
11. Liu, Y.; Liu, Y.; Li, J.; Sun, C.; Xu, W.; Zhao, B. Trajectory of coastal wetland vegetation in Xiangshan Bay, China, from image time series. *Mar. Pollut. Bull.* **2020**, *160*, 111697. [CrossRef]
12. Wang, X.; Xiao, X.; Zou, Z.; Hou, L.; Qin, Y.; Dong, J.; Doughty, R.B.; Chen, B.; Zhang, X.; Chen, Y.; et al. Mapping coastal wetlands of China using time series Landsat images in 2018 and Google Earth Engine. *ISPRS J. Photogramm. Remote Sens.* **2020**, *163*, 312–326. [CrossRef]
13. Zhang, S.; Yang, X.; Li, D.; Li, S.; Chen, Z.; Wu, J. A meta-analysis of understory plant removal impacts on soil properties in forest ecosystems. *Geoderma* **2022**, *426*, 116116. [CrossRef]
14. Qin, Y.; Xiao, X.; Wigneron, J.-P.; Ciais, P.; Canadell, J.G.; Brandt, M.; Li, X.; Fan, L.; Wu, X.; Tang, H.; et al. Large loss and rapid recovery of vegetation cover and aboveground biomass over forest areas in Australia during 2019–2020. *Remote Sens. Environ.* **2022**, *278*, 113087. [CrossRef]
15. Ottinger, M.; Clauss, K.; Kuenzer, C. Aquaculture: Relevance, distribution, impacts and spatial assessments—A review. *Ocean Coast. Manag.* **2016**, *119*, 244–266. [CrossRef]
16. Sun, Z.; Luo, J.; Yang, J.; Yu, Q.; Zhang, L.; Xue, K.; Lu, L. Nation-Scale Mapping of Coastal Aquaculture Ponds with Sentinel-1 SAR Data Using Google Earth Engine. *Remote Sens.* **2020**, *12*, 3086. [CrossRef]
17. Duan, Y.; Li, X.; Zhang, L.; Chen, D.; Liu, S.; Ji, H. Mapping national-scale aquaculture ponds based on the Google Earth Engine in the Chinese coastal zone. *Aquaculture* **2020**, *520*, 734666. [CrossRef]
18. Duan, Y.; Tian, B.; Li, X.; Liu, D.; Sengupta, D.; Wang, Y.; Peng, Y. Tracking changes in aquaculture ponds on the China coast using 30 years of Landsat images. *Int. J. Appl. Earth Obs. Geoinf.* **2021**, *102*, 102383. [CrossRef]
19. Li, N.; Niu, S.; Guo, Z.; Wu, L.; Zhao, J.; Min, L.; Ge, D.; Chen, J. Dynamic Waterline Mapping of Inland Great Lakes Using Time-Series SAR Data From GF-3 and S-1A Satellites: A Case Study of DJK Reservoir, China. *IEEE J. Sel. Top. Appl. Earth Obs. Remote Sens.* **2019**, *12*, 4297–4314. [CrossRef]
20. Fujiki, S.; Okada, K.; Nishio, S.; Kitayama, K. Estimation of the stand ages of tropical secondary forests after shifting cultivation based on the combination of World View-2 and time-series Landsat images. *ISPRS J. Photogramm. Remote Sens.* **2016**, *119*, 280–293. [CrossRef]
21. Wang, L.; Sousa, W.P.; Gong, P.; Biging, G.S. Comparison of IKONOS and Quick Bird images for mapping mangrove species on the Caribbean coast of Panama. *Remote Sens. Environ.* **2004**, *91*, 432–440. [CrossRef]
22. Cheng, B.; Liang, C.; Liu, X.; Liu, Y.; Ma, X.; Wang, G. Research on a novel extraction method using Deep Learning based on GF-2 images for aquaculture areas. *Int. J. Remote Sens.* **2020**, *41*, 3575–3591. [CrossRef]
23. Ottinger, M.; Bachofer, F.; Huth, J.; Kuenzer, C. Mapping Aquaculture Ponds for the Coastal Zone of Asia with Sentinel-1 and Sentinel-2 Time Series. *Remote Sens.* **2021**, *14*, 153. [CrossRef]
24. Duan, Y.; Li, X.; Zhang, L.; Liu, W.; Liu, S.; Chen, D.; Ji, H. Detecting spatiotemporal changes of large-scale aquaculture ponds regions over 1988–2018 in Jiangsu Province, China using Google Earth Engine. *Ocean. Coast. Manag.* **2020**, *188*, 105144. [CrossRef]
25. Yang, J.; Huang, X. The 30 m annual land cover dataset and its dynamics in China from 1990 to 2019. *Earth Syst. Sci. Data* **2021**, *13*, 3907–3925. [CrossRef]
26. Stiller, D.; Ottinger, M.; Leinenkugel, P. Spatio-temporal patterns of coastal aquaculture derived from Sentinel-1 time series data and the full Landsat archive. *Remote Sens.* **2019**, *11*, 1707. [CrossRef]
27. Prasad, K.; Ottinger, M.; Wei, C.; Leinenkugel, P. Assessment of Coastal Aquaculture for India from Sentinel-1 SAR Time Series. *Remote Sens.* **2019**, *11*, 357. [CrossRef]
28. Konapala, G.; Kumar, S.V.; Khalique Ahmad, S. Exploring Sentinel-1 and Sentinel-2 diversity for flood inundation mapping using deep learning. *ISPRS J. Photogramm. Remote Sens.* **2021**, *180*, 163–173. [CrossRef]
29. Drusch, M.; Del Bello, U.; Carlier, S.; Colin, O.; Fernandez, V.; Gascon, F.; Hoersch, B.; Isola, C.; Laberinti, P.; Martimort, P.; et al. Sentinel-2: ESA's Optical High-Resolution Mission for GMES Operational Services. *Remote Sens. Environ.* **2012**, *120*, 25–36. [CrossRef]
30. Geudtner, D.; Torres, R.; Snoeij, P.; Davidson, M.; Rommen, B. Sentinel-1 System capabilities and applications. In Proceedings of the 2014 IEEE Geoscience and Remote Sensing Symposium, Quebec City, QC, Canada, 13–18 July 2014; pp. 1457–1460.
31. Arvor, D.; Daher, F.R.G.; Briand, D.; Dufour, S.; Rollet, A.-J.; Simões, M.; Ferraz, R.P.D. Monitoring thirty years of small water reservoirs proliferation in the southern Brazilian Amazon with Landsat time series. *ISPRS J. Photogramm. Remote Sens.* **2018**, *145*, 225–237. [CrossRef]
32. Obida, C.B.; Blackburn, G.A.; Whyatt, J.D.; Semple, K.T. River network delineation from Sentinel-1 SAR data. *Int. J. Appl. Earth Obs. Geoinf.* **2019**, *83*, 101910. [CrossRef]
33. Amitrano, D.; Di Martino, G.; Iodice, A.; Riccio, D.; Ruello, G. Unsupervised Rapid Flood Mapping Using Sentinel-1 GRD SAR Images. *IEEE Trans. Geosci. Remote Sens.* **2018**, *56*, 3290–3299. [CrossRef]
34. Xia, Z.; Guo, X.; Chen, R. Automatic extraction of aquaculture ponds based on Google Earth Engine. *Ocean. Coast. Manag.* **2020**, *198*, 105348. [CrossRef]
35. Ottinger, M.; Clauss, K.; Kuenzer, C. Large-Scale Assessment of Coastal Aquaculture Ponds with Sentinel-1 Time Series Data. *Remote Sens.* **2017**, *9*, 440. [CrossRef]

36. Veettil, B.K.; Quang, N.X.; Trang, N.T.T. Changes in mangrove vegetation, aquaculture and paddy cultivation in the Mekong Delta: A study from Ben Tre Province, southern Vietnam. *Estuar. Coast. Shelf Sci.* **2019**, *226*, 106273. [CrossRef]
37. Affairs, Administration of Fisheries and Fisheries Administration of the Ministry of Agriculture and Rural, China. *China Fishery Yearbook*; China Agricultural Press: Beijing, China, 2020.
38. Pekel, J.-F.; Cottam, A.; Gorelick, N.; Belward, A.S. High-resolution mapping of global surface water and its long-term changes. *Nature* **2016**, *540*, 418–422. [CrossRef]
39. Jia, S.; Xue, D.; Li, C.; Zheng, J.; Li, W. Study on new method for water area information extraction based on Sentinel—1 data. *Yangtze River* **2019**, *50*, 213–217.
40. Otsu, N. A Threshold Selection Method from Gray-Level Histograms. *IEEE Trans. Syst. Man Cybern.* **1979**, *9*, 62–66. [CrossRef]
41. Senwen, W.C.H. Spatial-Temporal Changes in Aquaculture Ponds in Coastal Cities of Guangdong Province: An Empirical Study Based on Sentinel-1 Data during 2015–2019. *Trop. Geogr.* **2021**, *41*, 622–634. [CrossRef]
42. Ke, W.; Huanmei, Y.; Yi, H.; Huaquan, C.; Pengren, L. Remote sensing image extraction for coastal aquaculture ponds in the Guangxi Beibu Gulf based on Google Earth Engine. *Trans. Chin. Soc. Agric. Eng.* **2021**, *37*, 280–288. [CrossRef]